NIH Public Access
Author Manuscript
Biochim Biophys Acta. Author manuscript; available in PMC 2014 February 01.

Published in final edited form as:
Biochim Biophys Acta. 2013 February ; 1831(2): . doi:10.1016/j.bbalip.2012.10.010.

The glycolipid transfer protein (GLTP) domain of phosphoinositol 4-phosphate adaptor protein-2 (FAPP2): Structure drives preference for simple neutral glycosphingolipids

Ravi Kanth Kamlekar[a,1], **Dhirendra K. Simanshu**[b,1], **Yong-guang Gao**[a], **Roopa Kenoth**[a], **Helen M. Pike**[a], **Franklyn G. Prendergast**[c], **Lucy Malinina**[d], **Julian G. Molotkovsky**[e], **Sergei Yu Venyaminov**[c], **Dinshaw J. Patel**[b,*], and **Rhoderick E. Brown**[a,**]

[a]The Hormel Institute, University of Minnesota, Austin, MN, USA

[b]Memorial Sloan-Kettering Cancer Center, New York, NY, USA

[c]Mayo Clinic College of Medicine, Rochester, MN, USA

[d]CIC BioGUNE, Parque Tecnológico de Vizcaya, Derio 48160, Spain

[e]Shemyakin-Ovchinnikov Institute of Bioorganic Chemistry, Moscow 117997, Russia

Abstract

Phosphoinositol 4-phosphate adaptor protein-2 (FAPP2) plays a key role in glycosphingolipid (GSL) production using its C-terminal domain to transport newly synthesized glucosylceramide away from the cytosol-facing glucosylceramide synthase in the cis-Golgi for further anabolic processing. Structural homology modeling against human glycolipid transfer protein (GLTP) predicts a GLTP-fold for FAPP2 C-terminal domain, but no experimental support exists to warrant inclusion in the GLTP superfamily. Here, the biophysical properties and glycolipid transfer specificity of FAPP2-C-terminal domain have been characterized and compared with other established GLTP-folds. Experimental evidence for a GLTP-fold includes: *i*) far-UV circular dichroism (CD) showing secondary structure with high alpha-helix content and a low thermally-induced unfolding transition (~41 °C); *ii*) near-UV-CD indicating only subtle tertiary conformational change before/after interaction with membranes containing/lacking glycolipid; *iii*) Red-shifted tryptophan (Trp) emission wavelength maximum (λ_{max}~352 nm) for apo-FAPP2-C-terminal domain consistent with surface exposed intrinsic Trp residues; *iv*) 'signature' GLTP-fold Trp fluorescence response, i.e., intensity decrease (~30%) accompanied by strongly blue-shifted λ_{max} (~14 nm) upon interaction with membranes containing glycolipid, supporting direct involvement of Trp in glycolipid binding and enabling estimation of partitioning affinities. A structurally-based preference for other simple uncharged GSLs, in addition to glucosylceramide, makes human FAPP2-GLTP more similar to fungal HET-C2 than to plant AtGLTP1 (glucosylceramide-specific) or to broadly GSL-selective human GLTP. These findings along with the distinct mRNA exon/intron organizations originating from single-copy genes on separate human chromosomes suggest adaptive evolutionary divergence by these two GLTP-folds.

© 2012 Elsevier B.V. All rights reserved.

*Corresponding author. pateld@mskcc.org (D.J. Patel). **Correspondence to: R.E. Brown, Univ. of Minnesota, Hormel Inst, 801 16th Avenue NE, Austin, MN 55912, USA. Tel.: +1 507 437 9625; fax: +1 507 437 9606. reb@umn.edu (R.E. Brown).
[1]Authors contributing equally to this study.

Appendix A. Supplementary Data
Supplementary data to this article can be found online at http://dx.doi.org/10.1016/j.bbalip.2012.10.010.

NIH-PA Author Manuscript
NIH-PA Author Manuscript
NIH-PA Author Manuscript

NIH-PA Author Manuscript

NIH-PA Author Manuscript

NIH-PA Author Manuscript

Keywords

Glycosphingolipid binding and transfer; GLTP superfamily; Membrane interaction; Tryptophan fluorescence; Near-UV and far-UV circular dichroism; Divergent evolution

1. Introduction

The trans-Golgi network (TGN) functions as a major cell sorting complex, directing newly synthesized proteins and lipids to various subcellular destinations, receiving extracellular materials, and recycling molecules from endocytic compartments [1-3]. The exceptionally complex TGN sorting process involves mechanisms that regulate multiple divergent pathways to various acceptor compartments. Transport vesicle formation for various cargos involves attachment of distinct sets of docking and fusion factors (e.g. SNAREs) that target the correct acceptor compartment as well as the association of specific proteins that engage cytoskeletal tracks for vectorial trafficking. The maturation of transport vesicles destined for the plasma membrane often involves phosphoinositol 4-phosphate adaptor protein-2 (FAPP2) which uses its N-terminal pleckstrin homology domain to bind to phosphatidylinositol 4-phosphate in ADP-ribosylation-factor (ARF) dependent fashion and dock with Golgi membranes [4-8].

FAPP2 possesses a C-terminal domain with sequence homology to human glycolipid transfer protein (GLTP) [4,9,10]. This domain enables FAPP2 to transfer glucosylceramide (GlcCer) between cellular compartments. However, unlike GLTP (209 a.a.), FAPP2 (519 a.a.) contains an N-terminal pleckstrin homology (PH) domain that helps to target the Golgi. D'Angelo et al. [11] have reported that complex glycosphingolipid (GSL) synthesis relies on FAPP2-mediated transfer of GlcCer from its synthetic site on the cytoplasmic face of the cis-Golgi to the trans-Golgi compartment. In contrast, Halter et al. [12] suggest that FAPP2 transfers GlcCer from the trans-Golgi to the endoplasmic reticulum before GlcCer returns to the Golgi for complex GSL synthesis. In any case, having two glycolipid transfer proteins, FAPP2 and GLTP, able to access cytosolic-facing membranes is important for maintaining cell viability. In vivo siRNA silencing that knocks down FAPP2 fails to block the arrival of newly synthesized GlcCer at the plasma membrane in the presence of the vesicle trafficking disruptor, brefeldin A, suggesting partial redundancy of GlcCer transfer by GLTP which is also able to deliver GlcCer to the plasmamembrane in the presence of brefeldin A [12,13]. However, RNAi knockdown of both FAPP2 and GLTP results in cell death, suggesting a pivotal need for their functionality as glycolipid nonvesicular trafficking and/or sensor devices in cells. Downregulation of human FAPP2 gene (*PLEKHA8*; chromosome 7; locus 7p21-p11.2) by either target validation ribozymes or by FAPP2 siRNA also sensitizes cells to Fas/FasL-mediated apoptosis, emphasizing the need for normal FAPP2 expression to maintain cell viability and homeostasis [14].

Structural homology modeling of the FAPP2-C-terminal domain against the X-ray structure of human GLTP [15-17] predicts a GLTP-fold and topological conservation of key residues involved in glycolipid binding [10,11]. Yet, experimental data validating the FAPP2-C-terminal domain to be a GLTP-fold is lacking. Also, the exclusive focus on conserved core residues needed for sugar headgroup binding by the glycolipid recognition center without attention to residues that control GSL selectivity as well as transfer testing only of GlcCer and no other GSLs leave important issues unaddressed. Does the human FAPP2-C-terminal domain contain a GLTP-fold that has been evolutionarily adapted to transfer only GlcCer as reportedly occurs for plant GLTP1? Does transfer duplicity of human FAPP2 and human GLTP extend beyond GlcCer to include other glycolipids? In FAPP2, does the C-terminal domain structure or targeting by the N-terminal PH domain regulate glycolipid selectivity?

NIH-PA Author Manuscript

NIH-PA Author Manuscript

NIH-PA Author Manuscript

Herein, we have experimentally evaluated GLTP-fold formation by the FAPP2-C-terminal domain, determined its ability to transfer GSLs other than GlcCer, and identified local conformational changes expected to impact glycolipid binding specificity. Our experimental characterization includes assessment of intrinsic tryptophan fluorescence including 'signature' changes in intensity and emission wavelength maxima characteristic of GLTP-folds upon glycolipid binding as well as far-UV and near-UV CD spectroscopy to establish folding conformation, thermal stability, and changes induced by membrane interaction. Structural homology modeling against X-ray structures of human GLTP and fungal HET-C2 GLTP-fold [15,18] reveals local conformational changes expected to impact FAPP2 glycolipid selectivity. The results are discussed within the context of FAPP2 subcellular localization and evolutionary constraints imposed by the topology of GSL production and localization within cells.

2. Material and methods

2.1. Materials

1-Palmitoyl-2-oleoyl-*sn*-glycero-3-phosphocholine (POPC), dipalmitoyl phosphatidic acid (DPPA), and all sphingolipids were obtained from Avanti Polar Lipids (Alabaster, Al) except for ganglioside GM_1 which was purified as described previously [19]. Radiolabeled galactosylceramide (GalCer; [galactose-6-^{3}H]; 20 Ci/mmol), glucosylceramide (GlcCer; [stearoyl-1-^{14}C]; 50 mCi/mmol), and sulfatide ([stearoyl-1-^{14}C]; 50 mCi/mmol) were purchased from American Radiolabeled Chemicals (Saint Louis, MO). Tritiated GM_1 and LacCer were prepared using galactose oxidase and tritiated borohydride and purified as described previously [19,20]. N-[(11*E*)-12-(9-anthryl)-11-dodecenoyl]-1-O-β-galactosylsphingosine (AV-GalCer) [21] and 1-acyl-2-[9-(3- perylenoyl)-nonanoyl]-*sn*-glycero-3-phosphocholine (Per-PC) were synthesized as detailed earlier [22]. Stock concentrations of phospholipids were quantitated by phosphate determination [23] and of glycolipids, by gravimetric analyses [24].

2.2. Methods

2.2.1. Cloning, expression and purification—FAPP2 encoded by human *PLEKHA8* was cloned from human brain cDNA (Clontech) by PCR using Herculase® II Fusion DNA polymerase (or Pfu Ultra High Fidelity DNA polymerase), forward primer 5′-GGA AGC GGA AAG ATG GAG GGG GTG CTG TAC AAG TGG-3′ and reverse primer 5′-GA GGA GAA GCC CGG TCA TAC CAC CTC ATC AGA TTC CAG-3′. Amplified ORF encoding FAPP2 (519 a.a.; identical with GenBank GI:119614336) served as template for cloning the C-terminal domain (212 a.a. = FAPP2-C212). Insertion at the BamHI and SalI restriction sites into pET-28 (kanamycin resistant; Novagen) modified with small ubiquitin-like modifier (SUMO) protein ORF enabled heterologous expression using transformed Rosetta cells grown in Luria–Bertanimedium at 37 °C for 6 h, induced with 0.1 mM IPTG, and then grown 16–20 h at 20 °C. Purification from soluble lysate was achieved by Ni-NTA affinity chromatography. 6×His–SUMO-tag was removed from the N-terminus of FAPP2-C212 using a SUMO-specific protease, yielding a sequence identical to native protein. Final purification by FPLC SEC using a HiLoad 16/60 Superdex-75 prep grade column (Amersham) was verified by SDS-PAGE [20,25].

2.2.2. Protein concentration determination—A DU 640 spectrophotometer (Beckman) at a spectral bandwidth of 1.8 nm was used and the molar absorptivity was obtained by averaging the results from four calculation methods [26-29]. Spectra were corrected for turbidity by plotting the log dependence of the solution absorbance versus the log of the wavelength and extrapolating their linear dependence in the 340–440 nm to the 240–300 nm absorption range, using the DU-640 scatter correction routine. Extrapolated

NIH-PA Author Manuscript

NIH-PA Author Manuscript

NIH-PA Author Manuscript

absorbance values were subtracted from the measured values, decreasing the apparent protein absorbance at 280 nm by ~15%.

2.2.3. Circular dichroism spectroscopy—CD spectra of FAPP2-C212 (~50 μM) were collected in 10 mM sodium phosphate (pH 7.4), and 30 mM NaCl at 10 °C while continuously purging with N_2 using a J810 spectropolarimeter (JASCO, Japan) equipped with a CTC-345 temperature-control system. CD spectra were recorded using ten accumulations, scanning each at 20 nm/min with a 2 s response time as detailed previously [18,30,31 & references therein] and presented in units of molar ellipticity per residue. Secondary structure was calculated from far-UV spectra using DichroWeb on-line analysis [32,33].

2.2.4. 3D-structural homology modeling—FAPP2-GLTP was analyzed using 3D-Jigsaw and I-TASSER comparative modeling algorithms, which build 3D-protein models based on homologs of known structure [34,35].

2.2.5. Fluorescence spectroscopy—Trp fluorescence was selectively monitored by excitation at 295 nm and measuring emission (310 to 420 nm) at 25 °C using a SPEX FluoroMax spectrofluorometer (Horiba Scientific, Edison NJ) as performed previously [18,25,30]. Band passes for excitation and emission were 5 nm. The cuvette was temperature-controlled to ±0.1 °C (Neslab RTE-111, Thermo Fisher, Waltham, MA). For membrane interaction studies, the emission signals of FAPP2-GLTP (1 μM) were measured before and after addition of various amounts of POPC vesicles lacking or containing 20 mole% glycolipid. Spectra were corrected by subtraction of buffer blanks. Inner filter effects were avoided by keeping the protein concentration at OD_{295}<0.1.

2.2.6. Membrane vesicle preparation—Lipid mixtures, dissolved in dichloromethane, were dried under a gentle nitrogen stream. Remaining traces of solvent were removed by vacuum desiccation for >3 h. The dried lipid film was hydrated by vortexing for 5 min with 10 mM phosphate buffered saline (pH 7.4). Small unilamellar vesicles (SUVs) were prepared by probe sonication for 30–45 min using intermittent pulses of 2–3 min duration [36,37]. Residual multilamellar vesicles and titanium probe particles were removed by centrifugation at 100,000 *g* for 90 min. Size exclusion chromatography analysis confirmed average diameters of ~25–30 nm for SUVs.

2.2.7. Binding/partition coefficient analyses—Because glycolipid binding to FAPP2-C212 induced a dramatic λ_{max} blue-shift (351 to ~337 nm), intensity changes at 357 nm were used for binding isotherms to avoid problems discussed by White and colleagues [38]. The fraction of binding sites (α) occupied by glycolipids was calculated by Eq. (1) [39]:

$$\alpha=(F-F\mathrm{o})/F_{\max} \quad (1)$$

where *F*o and *F* are the Trp emission intensities of GLTP in the absence and presence of glycolipid, respectively, and F_{max} is the emission intensity of the fully liganded GLTP, i.e. at excess glycolipid. F_{max} was determined by plotting $1/(F-F\mathrm{o})$ vs. $1/L$ and extrapolating $1/L=0$, where *L* equals the total glycolipid concentration. ΔF_m (maximum fluorescence change when protein is completely saturated with glycolipid) was determined by plotting $1/L$ (glycolipid concentration) and $1/\Delta F$ (decrease in fluorescence intensity). The concentration of bound glycolipid was calculated using the relationship:

$$[\text{Bound lipid}]=\text{protein conc.}\times\Delta F/\Delta F_{\mathrm{m}}. \quad (2)$$

NIH-PA Author Manuscript

NIH-PA Author Manuscript

NIH-PA Author Manuscript

The free lipid concentration was calculated as:

$$[\text{Free lipid}]=[\text{Total lipid}]-[\text{Bound lipid}]. \quad (3)$$

K_d values shown in Table 2 were determined by least-squares (NLLSQ) fitting of the plot of bound lipid vs. free lipid. NLLSQ analyses and data simulations were performed with OriginPro 7.0 software (MicroCal, Northampton, MA). Nonlinear regression of the hyperbolic fit of the saturation isotherm avoided errors associated with linear transformations, i.e. Scatchard analysis.

2.2.8. Glycolipid transfer activity—FAPP2-GLTP glycolipid intermembrane transfer activity was measured by two established assays [36,37,40-42]. Radiolabeled glycolipid intervesicular transfer was assayed using negatively-charged donor vesicles (10 mol% DPPA in POPC) containing 2 mole% glycolipid (GalCer, GlcCer, LacCer, sulfatide, GM_1) and POPC acceptor vesicles (10-fold excess) incubated with FAPP2-GLTP (1 μg/ml) at 25 °C. Glycolipid transfer was quantified by liquid scintillation counting of acceptor vesicles eluted from DEAE minicolumns [36,37]. Förster resonance energy transfer (FRET) enabled continuous real-time monitoring of glycolipid transfer activity. The FRET assay involves mixing of POPC donor vesicles (formed by rapid ethanol injection) containing anthrylvinyl (AV)-labeled glycolipid (1 mole%) and nontransferable perylenoyl-labeled-PC (1.5 mole%) with POPC acceptor vesicles (formed by sonication) [40-42] and protein (1 μg/ml) at 25 °C. Recovery of emission intensity at 425 nm (AV-GalCer; excitation at 370 nm) occurs during protein-mediated transfer to POPC acceptor vesicles. No signal change is observed in the absence of POPC acceptor vesicles. In competition assays [42], glycolipids with naturally-occurring hydrocarbon chains were also included at 0.5 mole% in donor vesicles. Fitting to first-order exponential behavior and transfer rate calculation have been detailed previously [41].

3. Results

3.1. FAPP2-C212 conformation

Fig. 1A shows the sequence homology of FAPP2 C-terminal region compared to human GLTP and fungal HET-C2 and illustrates the conservation of the five core residues needed for GSL binding (yellow highlights) [11,15,18]. Because full-length FAPP2 displayed a strong tendency to self aggregate that adversely affected experimental characterization, several truncated FAPP2 forms were cloned and screened. A truncated FAPP2 consisting of the C-terminal 212 a.a. residues (FAPP2-C212) met the criteria of good solubility, no self-aggregation, and unmitigated transfer activity (see Supplemental information). Experimental insights into the secondary and tertiary conformations of FAPP2-C212 as well as its folding stability were provided by circular dichroic (CD) spectroscopic analyses in the far-UV (190–250 nm) and near-UV (250–320 nm) spectral regions. As expected for a GLTP-fold, the secondary structure of FAPP2-C212 contained substantial amounts of α-helix (Fig. 1B & Table 1) but not quite as extensive as GLTP or HET-C2 [18,30,31]. Because GLTP-folds have low unfolding temperatures (e.g. HET-C2 at ~49 °C; GLTP at ~54 °C), FAPP2-C212 conformational stability was tested. Fig. 1C shows a thermal scan of the first derivative of the far-UV CD signal at 222 nm, a wavelength choice dictated by α-helical proteins having a strong 222 nm CD signal that decreases in intensity upon unfolding. For FAPP2-C212, increasing temperature resulted in a cooperative unfolding transition between 25 °C and 50 °C with a midpoint of ~40.5 °C. This low unfolding temperature mid-point is consistent with a lack of stabilization by intramolecular disulfides that is typical for GLTP-folds (Supplementary Fig. S1). Other potential contributing parameters, such as α-helix content and pI, are assessed in the Discussion section.

NIH-PA Author Manuscript

NIH-PA Author Manuscript

NIH-PA Author Manuscript

The presence of two Trp, six Tyr, and 11 Phe residues in FAPP2-C212 suggested that near-UV CD measurements could prove useful for gaining insights into tertiary conformation. When the local environment induces optical activity in aromatic side chains of a protein, Tyr and Trp residues can generate signals in the 270–300 nm range and Phe residues can give rise to signals in the 255 to 270 nm range [43-45]. Fig. 1D shows the near-UV signal response of FAPP2-C212 to be weak with negative peaks at 257, 262, and 268 nm probably arising from its 11 Phe residues as also occurs in GLTP (10 Phe) and HET-C2 (12 Phe). Discernible signals (275–290 nm) from the two Trp and six Tyr residues in FAPP2-C212 were lacking, a situation differing from GLTP (3 Trp, 10 Tyr) and HET-C2 (2 Trp, 4 Tyr) [18,30].

3.2. FAPP2-C212 interaction with membranes

Fig. 2A shows the far-UV CD signal of FAPP2-C212 after mixing with bilayer vesicles consisting of POPC, POPC/POPA, or POPC/POPA/GalCer. The data show that FAPP2-C212 secondary structures remains largely α-helical, albeit less than in soluble FAPP2-C212, upon mixing with membranes. Mixing of POPC vesicles with FAPP2-C212 had a stabilizing effect on the protein as shown by the slightly elevated unfolding temperature mid-point (T_m~41.2 °C) (Fig. 2B) versus 40.5 °C in the solution (Fig. 1C). When POPA (10 mole%) was included in the POPC vesicles, higher helicity loss (35%) was observed, consistent with an average shortening of all helical segments by ~one residue or loss of one entire helix. A significant lowering of the protein T_m (~32.7 °C) also occurred (Fig. 2B). POPA was of interest because negatively-charged phosphoglyceride at 10 mol% was previously shown to decrease GLTP-mediated glycolipid transfer rates by enhancing protein partitioning affinity to membranes [37,46]. Fig. 2B shows that including GalCer in the POPC/POPA vesicles not only reversed the destabilizing effect of POPA but also actually dramatically improved stabilization (T_m~43 °C) suggesting that GalCer was being bound by FAPP2-C212.

Fig. 2C shows that the conformational destabilization revealed by far-UV CD was not readily apparent in the near-UV CD signal (250–350 nm) which detects local changes in the induced environmental polarizibility for residues with aromatic side chains. Nonetheless, a small spectral dip can be observed in the 285–290 nm region typically associated with Trp when POPC or POPC/POPA vesicles are present. The spectral dip is not observed in the presence of POPC/POPA/GalCer vesicles or in the absence of vesicles, suggesting that the conformational change triggered during membrane interaction is rapidly reversed by glycolipid uptake.

Further insights into the conformational changes induced when FAPP2-C212 interacts with membranes and/or binds glycolipid were gained by investigating the intrinsic Trp fluorescence, a known environmental polarity indicator. The Trp emission wavelength maximum (λ_{max}) was 351 nm for apo-FAPP2-C212 (Fig. 3). This relatively red-shifted λ_{max} was consistent with the two Trp residues of FAPP2-C212 being freely exposed to the aqueous milieu. Red-shifted Trp λ_{max} responses are also displayed by apo-HET-C2 (354 nm) and apo-GLTP (348 nm) [18,25]. We hypothesized that, if the two Trp residues in FAPP2-C212 occupy similar conformational positions and function analogously to their GLTP counterparts, then the response of FAPP2-C212 Trp to membranes containing and lacking glycolipid should be similar to that of GLTP. To test the idea, vesicles consisting of POPC, POPC/GalCer (8:2), POPC/POPA (9:1), and POPC/POPA/GalCer (7:1:2) were added in stepwise increments to FAPP2-C212. Fig. 3 shows that addition of the POPC/GalCer or POPC/POPA/GalCer vesicles reduced the Trp emission intensity (~31%) and generated a substantial λ_{max} blue-shift (351→337 nm; 14-nm) (Table 3), a response similar to that triggered by glycolipid binding to human GLTP and HET-C2 [18,25,49]. It is noteworthy that the λ_{max} blue-shift ceases after a slight excess of glycolipid has been added,

NIH-PA Author Manuscript

NIH-PA Author Manuscript

NIH-PA Author Manuscript

but the intensity continues to incrementally decrease. In contrast, stepwise addition of POPC or POPC/POPA vesicles lacking glycolipid (Fig. 3A) produced almost no λ_{max} blue-shift (1 nm) and more moderate reduction in emission intensity (~19–22%). Also noteworthy was the similar response produced by vesicles containing either GalCer or GlcCer and the slightly weaker response produced by vesicles containing LacCer (Supplementary Fig. S2). Inclusion of sphingomyelin or ceramide elicited almost no λ_{max} blue-shift (data not shown), as also was the case for vesicles lacking glycolipid (Figs. 3A,B & S2A).

The Trp emission responses with membranes containing or lacking glycolipid suggested that both glycolipid binding and protein interaction with the membrane contribute to the overall signal response. Estimation of the membrane partition coefficient values (K_d values) of FAPP2-C212 yielded values of 10.6 μM for POPC vesicles, and 1.01 μM for POPC/GalCer vesicles (Table 2). The presence of PA (10 mole%) in the POPC and POPC/GalCer vesicles slightly enhanced the K_d values to 13.5 μM and 1.35 μM, respectively. The relatively weak membrane partitioning is consistent with FAPP2-C212 acting as a peripheral amphitropic membrane protein which reversibly translocates to/from membranes to function, i.e. transfer lipids between membranes. The lower K_d value observed when the vesicles contain glycolipid supports the presence of Trp within the glycolipid binding site of FAPP2-C212.

3.3. FAPP2-C212 is a glycolipid transfer protein

We assessed FAPP2-C212 functionality for glycolipid transfer by monitoring the Förster resonance energy transfer (FRET) response of POPC membrane (donor vesicles) containing anthrylvinyl (AV)-labeled glycolipid (1 mole%) and nontransferable perylenoyl-labeled-PC (1.5 mole%) as a function of time in the presence of catalytic amounts of FAPP2-C212 (Fig. 4A). The increase in AV emission intensity, reflecting removal of AV-glycolipid from donor vesicles, was apparent only if POPC acceptor vesicles were present, consistent with the intervesicular transfer of the glycolipid rather than just glycolipid binding by FAPP2-C212. The dramatic slow-down in the exponential kinetic time course of AV-glycolipid transfer after ~11 min appears to reflect exhaustion of available AV-glycolipid ‘substrate’ in the outer monolayer of the membrane because addition of excess detergent (Tween 20) results in a sudden and dramatic increase in AV-GalCer emission. The detergent-induced solubilization enables ‘infinite’ separation of the AV-GalCer and perylenoyl PC and provides an indication of the maximal AV emission possible. Fig. 4A shows that the AV-GalCer pool accessible to FAPP2-C212 is limited to ~50%, the known outer leaflet distribution for GalCer in vesicles [40,41]. The lack of all AV-GalCer being accessible in the donor vesicles is consistent with FAPP2-C212 being an amphitropic peripheral protein that interacts with membrane surfaces without penetrating sufficiently to access glycolipid ‘substrate’ in the membrane inner leaflet or promote rapid flipping of glycolipid ‘substrate’ to the outer leaflet of the membrane.

The ability of FAPP-C212 to function as a bona fide glycolipid transfer protein was also confirmed using radiolabeled glycolipids (Supplementary Fig. S3). Because low glycolipid concentrations are typical of biomembranes, the donor vesicles contained only 2 mole% GalCer in POPC. Estimates of the first order transfer rate at 30 °C were ~3.5 pmol GalCer transferred per min per FAPP-GLTP molecule (Supplementary Fig. S3, lower panel). The rate compares favorably with the transfer rate of dehydroergosterol by STARD4 at 37 °C from donor vesicles containing 23 mole% dehydroergosterol [50]. It is noteworthy that, despite the reported sequence similarity between GLTP and the C-terminal region of FAPP2, many FAPP2 clones failed to show glycolipid transfer activity (see Supplemental information).

Competition analyses were performed to assess whether FAPP2-C212 prefers certain molecular species of monoglycosylceramides. By including nonfluorescent glycolipids with

NIH-PA Author Manuscript

NIH-PA Author Manuscript

NIH-PA Author Manuscript

naturally-occurring acyl chains along with fluorescent glycolipid in the donor vesicles, the slowdown in AV-glycolipid transfer kinetics could be assessed [e.g. 42]. As shown by Fig. 4A and B, 16:0 GalCer, 18:0 GalCer, and 24:0 GalCer compete slightly better than 12:0 GalCer, 18:1 GalCer, or 24:1 GalCer. Thus, FAPP2-C212, like GLTP, is able to accommodate GSLs containing a broad spectrum of acyl chains in their ceramide moieties.

3.4. Lipid transfer specificity of FAPP2-C212

As noted earlier, GlcCer was the only glycolipid tested when FAPP2 was reported to be a GlcCer transfer protein [11], leaving the issue of FAPP2's ability to transfer of other glycosphingolipids unanswered. Fig. 4C shows the transfer of different radiolabeled glycolipids by FAPP2-C212. In addition to GlcCer, GalCer and LacCer are readily transferred, a pattern also observed with GLTP and HET-C2. However, like HET-C2, FAPP2-C212 was unable to transfer negatively-charged glycolipids such as sulfatide and ganglioside GM_1 even though GLTP transfers these lipids quite well. Thus, the overall transfer specificity of human FAPP2-C212 more closely resembles fungal HET-C2 [18] rather than mammalian GLTP [10].

4. Discussion

4.1. FAPP2-C-terminal domain is a GLTP-fold

In the present study, we have provided experimental evidence for the C-terminal domain of FAPP2 forming a bona fide GLTP-fold with more focused glycolipid selectivity than human GLTP, but not exclusively specific for GlcCer. Fluorescence emission of the intrinsic Trp residues in FAPP2-C212 in the absence/presence of glycolipid provides the most compelling experimental support for a GLTP-fold. The so-called 'signature' Trp emission response of a GLTP-fold, i.e. substantial decrease (~31%) in emission intensity and λ_{max} blue-shift (12 nm), is apparent upon incubation of apo-FAPP2-C212 with membrane vesicles containing glycolipid. A similar Trp emission response has been reported for two structurally validated GLTP-folds, GLTP and HET-C2, and arises from glycolipid binding [18,25,49]. Trp involvement in glycolipid binding in FAPP2-C212 is also supported by 3D-JigSaw and I-TASSER in silico structural homology analyses [34,35] performed after exhaustive, high through-put crystallization robotics for X-ray structural determinations were unfruitful. Fig. 5A shows the GLTP-fold predicted for FAPP2-C212 and the similar positioning of Trp^{407} in FAPP2, Trp^{96} in GLTP, and Trp^{109} in HET-C2 in relation to bound GlcCer [15,18,25,30,46-49]. By forming the bottom of the glycolipid headgroup recognition center, FAPP2 Trp^{407} is expected to serve as a stacking plate that facilitates hydrogen bonding of Asp^{360}, Asn^{364}, and Lys^{367} with the sugar headgroup while Asp^{360} and His^{445} act as hydrogen bond 'clip' that holds and orients the ceramide amide region of the glycolipid (Fig. 5B).

The other Trp residue of FAPP2-C212 (Trp^{447}) is predicted to reside on the surface of helix-6 in a similar location as GLTP Trp^{142} and HET-C2 Phe^{149} and function as an interfacial anchor during transient interaction with membranes [15,18,30,46-49]. Surface hydropathy analysis [51] reveals a high concentration of nonpolar residues adjacent to Trp^{447} along the cleft-like gate for glycolipid uptake, consistent with its function as the initial membrane docking site (Fig. 5C). Fig. 5D illustrates membrane docking of FAPP2-C212 as analyzed by the orientation of proteins in membranes (OPM) computational approach [52], which take protein surface hydrophobicity into account to aid in identification of potential membrane-binding sites [51,53]. Optimal rotational and translational positioning of the protein with respect to the lipid bilayer is achieved by minimization of the protein transfer energy from water to the membrane hydrocarbon core, approximated as decadiene nonpolar solvent, and to interfacial regions characterized by

NIH-PA Author Manuscript

NIH-PA Author Manuscript

NIH-PA Author Manuscript

water-permeation profiles. Protein partitioning to the membrane is driven by hydrophobic interactions and opposed by desolvation of polar and charged groups. OPM analyses indicate a membrane penetration depth of ~5.8±0.8 Å with a tilt angle of ~87±3° and $\Delta G_{transfer}$ of 9.8 kcal/mol for FAPP2-C212. The membrane docking site includes Trp^{447}, Val^{448}, Val^{449}, Val^{452}, Leu^{455}, and Arg^{458} of helix 6 and Met^{359} and Pro^{351} of the adjacent inter-helical loop that form a hydrophobic patch.

While the highly red-shifted fluorescence λ_{max} of apo-FAPP2-C212 attests to exposure of Trp to the aqueous environment as is known for other GLTP-folds, the change in Trp emission intensity and blue-shift in λ_{max} induced by membranes containing glycolipid provide insights into the FAPP2-C212 binding affinity for glycolipids embedded in membranes. The K_d values for vesicles containing various glycolipids indicate only moderate binding strength by FAPP2, consistent with a role in glycolipid transfer requiring partitioning on and off membranes wth relative ease. The K_d values also agree well with previous values for human GLTP and HET-C2 calculated from the Trp intensity decrease.

Despite the similarities in global conformation for GLTP, HET-C2, and FAPP2-C212, important differences exist. Thermal unfolding of FAPP2-C212 (T_m~41 °C) occurs at lower temperature compared to GLTP (T_m~53 °C) and HET-C2 (T_m~49 °C). The destabilization could reflect the differing helix content in FAPP2-C212 detected by CD spectral studies. However, it is also noteworthy that the isoelectric points calculated for FAPP2-C212 (pI 5.42), HET-C2 (pI 6.34), and GLTP (pI 6.92) using ExPASy ProtParam differ significantly. The lower unfolding temperature of FAPP2-C212 at pH 7.4 could reflect destabilization by salt bridge disruption and/or alterations in cation–pi interactions, especially those involving the five His residues. Structural mapping by X-ray diffraction or NMR will be needed for precise determination of the subtle conformational differences that exist for the GLTP-fold of FAPP2-C212 compared to GLTP and HET-C2. While structural homology modeling has proven to be reliable for ascertaining core conformational structures of related GLTP homologs, reliability is more limited for the GLTP-fold N- and C-terminal regions [e.g. 18].

4.2. Structural features of FAPP2-GLTP only partially explain the preference for GlcCer

The dual functional role of FAPP2 in both higher GSL synthesis and ADP-ribosylation-factor (ARF)-dependent maturation of Golgi transport vesicles destined for the plasma membrane [11] places special importance on understanding the workings of this amphitropic protein. During complex glycosphingolipid biosynthesis, FAPP2 transfers newly synthesized GlcCer away from the cytosol-facing GlcCer synthase in the Golgi [10-13]. Whether the preference for GlcCer is location-based (reflecting the glycolipid topology in subcellular membranes) or structurally-based has remained unclear for the following reasons: *i*) previous testing of FAPP2 transfer specificity involved GlcCer, sphingomyelin, ceramide, and PC, but no other glycolipids [11]; *ii*) previous structural homology modeling of the GLTP domain of FAPP2 focused on global folding topology and the positional conservation of the five core residues involved in glycolipid binding (Asp^{360}, Asn^{364}, Lys^{367}, Trp^{407}, His^{445}); *iii*) all characterized GLTP-folds (human GLTP, fungal HET-C2, and plant AtGLTP1) contain these same five conserved residues which anchor the glycolipid sugar-amide region into the sugar headgroup recognition center. Nonetheless, human GLTP displays broad selectivity for various glycolipids [18] while fungal HET-C2 and plant AtGLTP1 display much more focused transfer selectivity for simple neutral glycolipids [18,54]; *iv*) structural studies of HET-C2 [18] and homology modeling studies of AtGLTP1 [54] indicate that other nearby residues affect the local surface topology and charge, imparting subtle structural differences that generate the more focused glycolipid specificity of HET-C2 and AtGLTP1.

NIH-PA Author Manuscript

NIH-PA Author Manuscript

NIH-PA Author Manuscript

We found that FAPP2-C212 is not strongly biased for GlcCer but efficiently transfers other simple neutral glycosylceramides, i.e. GalCer, and LacCer. However, transfer is nearly completely abolished by addition of negatively-charged sulfate to GalCer, i.e. sulfatide. To elucidate the structural basis for the glycolipid selectivity by FAPP2-C212, sugar headgroup docking was performed using high resolution GLTP:GalCer and GLTP:LacCer complexes [15,16,42] as guides (Fig. 6A–C). In FAPP2-C212, the Trp^{407} indole group serves as a stacking platform that facilitates the hydrogen bonding of Asp^{360}, Asn^{364}, and Lys^{367} with Gal or Glc in the same way that Trp^{96} facilitates the hydrogen bonding network of Asp^{48}, Asn^{52}, and Lys^{55} with Gal or Glc in human GLTP [15,16,42]. However, in FAPP2-C212, the residue corresponding to Leu^{92} in GLTP is replaced by negatively-charged Glu^{403} in FAPP2. Docking of Glc, Gal, and Lac shows that Glu^{403} forms one H-bond with the 4OH group of Glc but none with Gal or Lac (Fig. 6A–C). In FAPP2, Arg^{398} forms one hydrogen bond with the 6OH group of Glc, Gal, and Glc (of Lac), thus serving a similar role as Tyr^{207} in GLTP [15,16,42]. Negatively-charged Glu^{403} appears to be well positioned to impede interaction with 3-sulfo-GalCer (sulfatide).

The structural basis for the more focused FAPP2-C212 glycolipid selectivity compared to human GLTP and fungal HET-C2 is illustrated in space-filling form by Fig. 7. Negatively-charged Glu^{403} may form a salt bridge with Lys^{367}, but is also well positioned to repel negatively-charged functional groups such as the sulfate of sulfo-GalCer, thereby interfering with its binding/transfer by FAPP2-C212. By contrast, nonpolar Leu^{92} occupies this same position in GLTP which proficiently binds and transfers sulfatide [42]. Other FAPP2-C212 residues (Val^{519}, Val^{397}, Arg^{398}, Asn^{399}, Ser^{400}) affect the protein surface topology adjacent to the glycolipid headgroup recognition center by providing steric bulk that narrows the headgroup interaction region compared to the ‘open trough’-like surface topology of the sugar headgroup binding region in GLTP. The constricted glycolipid headgroup recognition center in the FAPP2-C212 could explain the lack of interaction with branched, negatively-charged sugar headgroups, i.e. ganglioside GM_1. The net effect is a sugar recognition center better adapted for focused interaction with uncharged monohexosyl- and dihexosylceramides in human FAPP2-C212 compared to the broadly selective human GLTP.

The focused glycolipid selectivity and lack of sulfatide transfer by FAPP2-C212 are functional features shared with fungal HET-C2 [18]. However, the specificity is not nearly as focused as plant AtGLTP1 which reportedly transfers GlcCer much faster than GalCer (~8-fold) and LacCer (~32.5-fold), but not at all sphingomyelin [54]. The strong preference of AtGLTP1 for GlcCer is shared by neither FAPP2, GLTP nor HET-C2, which transfers GlcCer and GalCer at roughly similar rates. To explain the AtGLTP1 selectivity for GlcCer over GalCer, West et al. [54] proposed that the 4-hydroxyl in glucose, but not in galactose, is sufficiently close to interact with the amide group of Asn95 of AtGLTP1, the same site as Leu92 in human GLTP. It is noteworthy that this site is occupied by negatively-charged Glu in both FAPP2 and HET-C2.

From the molecular biological perspective, it is apparent that FAPP2 is encoded by single-copy *PLEKHA8* on human chromosome 7 (locus 7p21-p11.2). Mature *PLEKHA8* transcript contains 14 exons with the final 6 exons encoding most (202 a.a.) of the GLTP domain (see Supplemental information). By contrast, single-copy *GLTP* resides on human chromosome 12 (locus 12q24.11). Mature transcript arises by cis alternative splicing involving the 5 exons that encode the 209 a.a. protein [55]. The presence of two distinct genes, located on separate human chromosomes and encoding GLTP-folds that originate from different exon organizational patterns, attests to the biological utility and evolutionary importance of this protein fold.

NIH-PA Author Manuscript

NIH-PA Author Manuscript

NIH-PA Author Manuscript

It is intriguing that plant AtGLTP1 has evolved very high specificity for GlcCer [54]. Neither GalCer nor LacCer is present in plants, a situation that would presumably reduce evolutionary pressure for development of GlcCer-specific AtGLTP1. Because mammalian cells contain GlcCer, GalCer, and LacCer, evolutionary pressure to conserve the GlcCer-specific AtGLTP1 for use in FAPP2 is expected to be high. Nonetheless, the high GlcCer specificity of AtGLTP1 has not been conserved in FAPP2. Thus other factors must lessen the evolutionary pressure exerted by structure alone. One factor could be topological location of simple glycolipids that regulates their availability in cytosol-facing membranes and accessibility to FAPP2. In mammalian cells, GlcCer is produced by the cytosol-facing GlcCer synthase in the Golgi, but GalCer and LacCer are not normally found in cytosol-facing membranes. Another factor could be the targeting motifs such as the pleckstrin homology domain in FAPP2 that guide interaction to select subcellular sites (e.g. Golgi). In any case, it is also tempting to speculate that the lack of strong specificity of FAPP2 for GlcCer leaves open the possibility for interaction with other simple neutral GSLs if currently undiscovered events (pathological or normal) were to leave such glycolipids appropriately positioned and facing the cytosol.

Supplementary Material

Refer to Web version on PubMed Central for supplementary material.

Acknowledgments

We are grateful for the support by NIH/NIGMS GM45928 & GM34847, NIH/NCI CA121493, Spanish Ministerio de Ciencia e Innovacion (MICINN BFU2010-17711), Russian Foundation for Basic Research 012-04-00168; Abby Rockefeller Mauzé Trust, and the Dewitt Wallace, Maloris, Mayo, and Hormel Foundations. The molecular graphic images shown in Figs. 5, 7, and S1 were produced using UCSF Chimera (NIH P41 RR-01081) provided by the Resource for Biocomputing, Visualization, and Informatics at the University of California, San Francisco.

References

1. Rodriguez-Boulan E, Kreitzer G, Müsch A. Organization of vesicular trafficking in epithelia. Nat Rev Mol Cell Biol. 2005; 6:233–247. [PubMed: 15738988]
2. De Matteis MA, Luini A. Exiting the Golgi complex. Nat Rev Mol Cell Biol. 2008; 9:273–284. [PubMed: 18354421]
3. Graham TR, Burd CG. Coordination of Golgi functions by phosphatidylinositol 4-kinases. Trends Cell Biol. 2011; 21:113–121. [PubMed: 21282087]
4. Godi A, Di Campli A, Konstantakopoulos A, Di Tullio G, Alessi DR, Kular GS, Daniele T, Marra P, Lucocq JM, De Matteis MA. FAPPs control Golgi-to-cell-surface membrane traffic by binding to ARF and PtdIns(4)P. Nat Cell Biol. 2004; 6:393–404. [PubMed: 15107860]
5. Cao X, Coskun Ü, Rössle M, Buschhorn SB, Grzybek M, Dafforn TR, Lenoir M, Overduin M, Simons K. Golgi protein FAPP2 tubulates membranes. Proc Natl Acad Sci U S A. 2009; 106:21121–21125. [PubMed: 19940249]
6. Lenoir M, Coskun Ü, Grzybek M, Cao X, Buschhorn SB, James J, Simons K, Overduin M. Structural basis of wedging the Golgi membrane by FAPP pleckstrin homology domains. EMBO Rep. 2010; 11:279–284. [PubMed: 20300118]
7. Vieira OV, Verkade P, Manninen A, Simons K. FAPP2 is involved in the transport of apical cargo in polarized MDCK cells. J Cell Biol. 2005; 170:521–526. [PubMed: 16103222]
8. Donaldson JG, Jackson CL. ARF family G proteins and their regulators: roles in membrane transport development, and disease. Nat Rev Mol Cell Biol. 2011; 12:362–375. [PubMed: 21587297]
9. Brown RE, Mattjus P. Glycolipid transfer proteins. Biochim Biophys Acta. 2007; 1771:746–760. [PubMed: 17320476]

NIH-PA Author Manuscript

NIH-PA Author Manuscript

NIH-PA Author Manuscript

10. Mattjus P. Glycolipid transfer proteins and membrane interaction. Biochim Biophys Acta. 2009; 1788:267–272. [PubMed: 19007748]
11. D'Angelo G, Polishchuk E, Di Tullio G, Santoro M, Di Campli A, Godi A, West G, Bielawski J, Chuang C-C, van der Spoel AC, Platt FM, Hannun YA, Polishchuk R, Mattjus P, De Matteis MA. Glycosphingolipid synthesis requires FAPP2 transfer of glucosylceramide. Nature. 2007; 449:62–67. [PubMed: 17687330]
12. Halter D, Neumann S, van Dijk SM, Wolthoorn J, de Maziere AM, Vieira OV, Mattjus P, Klumperman J, vanMeer G, Sprong H. Pre- and post-Golgi translocation of glucosylceramide in glycosphingolipid synthesis. J Cell Biol. 2007; 179:101–115. [PubMed: 17923531]
13. Warnock DE, Lutz MS, Blackburn WA, Young WW Jr, Baenziger JU. Transport of newly synthesized glucosylceramide to the plasma membrane by a non-Golgi pathway. Proc Natl Acad Sci U S A. 1994; 91:2708–2712. [PubMed: 8146178]
14. Tritz R, Hickey MJ, Lin AH, Hadwiger P, Sah DWY, Neuwelt EA, Mueller BM, Kruse CA. FAPP2 gene downregulation increases tumor cell sensitivity to Fas-induced apoptosis. Biochem Biophys Res Commun. 2009; 383:167–171. [PubMed: 19341712]
15. Malinina L, Malakhova ML, Teplov A, Brown RE, Patel DJ. Structural basis for glycosphingolipid transfer specificity. Nature. 2004; 430:1048–1053. [PubMed: 15329726]
16. Malinina L, Malakhova ML, Kanack AT, Lu M, Abagyan R, Brown RE, Patel DJ. The liganding of glycolipid transfer protein is controlled by glycolipid acyl structure. PLoS Biol. 2006; 4:e362. [PubMed: 17105344]
17. Airenne TT, Kidron H, Nymalm Y, Nylund M, West GP, Mattjus P, Salminen TA. Structural evidence for adaptive ligand binding of glycolipid transfer protein. J Mol Biol. 2006; 355:224–236. [PubMed: 16309699]
18. Kenoth R, Simanshu DK, Kamlekar RK, Pike HM, Molotkovsky JG, Benson LM, Bergen HR, Prendergast FG, Malinina L, Venyaminov SY, Patel DJ, Brown RE. Structural determination and tryptophan fluorescence of heterokaryon incompatibility C2 protein (HET-C2), a fungal glycolipid transfer protein (GLTP), provide novel insights into glycolipid specificity and membrane interaction by the GLTP-fold. J Biol Chem. 2010; 285:13066–13078. [PubMed: 20164530]
19. Brown RE, Hyland KJ. Spontaneous transfer of ganglioside GM1 from its micelles to lipid vesicles of differing size. Biochemistry. 1992; 31:10602–10609. [PubMed: 1420175]
20. Malakhova ML, Malinina L, Pike HM, Kanack AT, Patel DJ, Brown RE. Point mutational analysis of the liganding site in human glycolipid transfer protein. Functionality of the complex. J Biol Chem. 2005; 280:26312–26320. [PubMed: 15901739]
21. Molotkovsky JG, Mikhalyov II, Imbs AB, Bergelson LD. Synthesis and characterization of newfluorescent glycolipid probes. Molecular organisation of glycosphingolipids in mixed-composition lipid bilayers. Chem Phys Lipids. 1991; 58:199–212.
22. Molotkovsky JG, Bergelson LD. Perylenoyl-labeled lipid-specific fluorescent probes. Bioorg Khim. 1982; 8:1256–1262.
23. Bartlett GR. Phosphorous assay in column chromatography. J Biol Chem. 1959; 234:466–468. [PubMed: 13641241]
24. Ali S, Brockman HL, Brown RE. Structural determinants of miscibility in surface films of galactosylceramide and phosphatidylcholine: effect of unsaturation in the galactosylceramide acyl chain. Biochemistry. 1991; 30:11198–11205. [PubMed: 1958657]
25. Li X-M, Malakhova ML, Lin X, Pike HM, Chung T, Molotkovsky JG, Brown RE. Human glycolipid transfer protein: probing conformation using fluorescence spectroscopy. Biochemistry. 2004; 43:10285–10294. [PubMed: 15287756]
26. Mihaly EJ. Numerical values of the absorbances of the aromatic amino acids in acid, neutral and alkaline solutions. Chem Eng Data. 1968; 13:179–182.
27. Gill SC, von Hippel PH. Calculation of protein extinction coefficients from amino acid sequence data. Anal Biochem. 1989; 182:319–326. [PubMed: 2610349]
28. Mach H, Middaugh CR, Lewis RV. Statistical determination of the average values of the extinction coefficients of tryptophan and tyrosine in native proteins. Anal Biochem. 1992; 200:74–80. [PubMed: 1595904]

NIH-PA Author Manuscript

NIH-PA Author Manuscript

NIH-PA Author Manuscript

29. Pace CN, Vajdos F, Fee L, Grimsley G, Gray T. How to measure and predict the molar absorption coefficient of a protein. Protein Sci. 1995; 4:2411–2423. [PubMed: 8563639]
30. Kamlekar R-K, Gao Y, Kenoth R, Pike HM, Molotkovsky JG, Prendergast FG, Malinina L, Patel DJ, Wessels W, Venyaminov SY, Brown RE. Human GLTP: three distinct functions for the three tryptophans in a novel peripheral amphitropic fold. Biophys J. 2010; 99:2626–2635. [PubMed: 20959104]
31. Kenoth R, Kamlekar R-K, Simanshu DK, Gao Y, Malinina L, Prendergast FG, Molotkovsky JG, Pathel DJ, Venyaminov SY, Brown RE. Conformational folding and stability of the HET-C2 glycolipid transfer protein fold: does a molten globule-lie state regulate activity? Biochemistry. 2011; 50:5163–5171. [PubMed: 21553912]
32. Whitmore L, Wallace BA. DICROWEB: an on-line server for protein secondary structure analyses from circular dichroism spectroscopic data. Nucleic Acids Res. 2004; 32:W668–W673. [PubMed: 15215473]
33. Whitmore L, Wallace BA. Protein secondary structure analyses from circular dichroism spectroscopy: methods and reference databases. Biopolymers. 2008; 89:392–400. [PubMed: 17896349]
34. Bates PA, Kelley LA, MacCallum RM, Sternberg MJE. Enhancement of protein modelling by human intervention in applying the automatic programs 3D-JIGSAW and 3D-PSSM. Proteins Struct Funct Genet Suppl. 2001; 5:39–46.
35. Roy A, Kucukural A, Zhang Y. I-TASSER: a unified platform for automated protein structure and function prediction. Nat Protoc. 2010; 5:725–738. [PubMed: 20360767]
36. Brown RE, Jarvis KL, Hyland KJ. Purification and characterization of glycolipid transfer protein from bovine brain. Biochim Biophys Acta. 1990; 1044:77–83. [PubMed: 2340310]
37. Mattjus P, Pike HM, Molotkovsky JG, Brown RE. Charged membrane surfaces impede the protein-mediated transfer of glycosphingolipids between phospholipid bilayers. Biochemistry. 2000; 39:1067–1075. [PubMed: 10653652]
38. Ladokhin AS, Jayasinghe S, White SH. How to measure and analyze tryptophan fluorescence in membranes properly and why bother? Anal Biochem. 2000; 285:235–245. [PubMed: 11017708]
39. Srivastava R, Ratheesh A, Gude RK, Rao KVK, Panda D, Subrahmanyam G. Resveratrol inhibits type II phosphatidylinositol 4-kinase: a key component in pathways of phosphoinositide turn over. Biochem Pharmacol. 2005; 70:1048–1055. [PubMed: 16102733]
40. Mattjus P, Molotkovsky JG, Smaby JM, Brown RE. A fluorescence resonance energy transfer approach for monitoring protein-mediated glycolipid transfer between vesicle membranes. Anal Biochem. 1999; 268:297–304. [PubMed: 10075820]
41. Rao CS, Lin X, Pike HM, Molotkovsky JG, Brown RE. Glycolipid transfer protein mediated transfer of glycosphingolipids between membranes: a model for action based on kinetic and thermodynamic analyses. Biochemistry. 2004; 43:13805–13815. [PubMed: 15504043]
42. Samygina VR, Popov AN, Cabo-Bilbao A, Ochoa-Lizarralde B, Goni-de-Cerio F, Zhai X, Molotkovsky JG, Patel DJ, Brown RE, Malinina L. Enhanced selectivity for sulfatide by engineered human glycolipid transfer protein. Structure. 2011; 19:1644–1654. [PubMed: 22078563]
43. Kelly SM, Jess TJ, Price NC. How to study proteins by circular dichroism. Biochim Biophys Acta. 2005; 1751:119–139. [PubMed: 16027053]
44. Venyaminov SY, Klimtchuk ES, Bajzer Z, Craig TA. Changes in structure and stability of calbindin-D28K upon calcium binding. Anal Biochem. 2004; 334:97–105. [PubMed: 15464957]
45. Craig TA, Benson LM, Bergen HR III, Venyaminov SY, Salisbury JL, Ryan ZC, Thompson JR, Sperry J, Gross ML, Kumar R. Metal-binding properties of human centrin-2 determined by micro-electrospray ionization mass spectrometry and UV spectroscopy. J Am Soc Mass Spectrom. 2006; 17:1158–1171. [PubMed: 16750384]
46. Rao CS, Chung T, Pike HM, Brown RE. Glycolipid transfer protein interaction with bilayer vesicles: modulation by changing lipid composition. Biophys J. 2005; 89:4017–4028. [PubMed: 16169991]
47. West G, Nylund M, Slotte JP, Mattjus P. Membrane interaction and activity of the glycolipid transfer protein. Biochim Biophys Acta. 2006; 1758:1732–1742. [PubMed: 16908009]

NIH-PA Author Manuscript

NIH-PA Author Manuscript

NIH-PA Author Manuscript

48. Neumann S, Opacić M, Wechselberger RW, Sprong H, Egmond MR. Glycolipid transfer protein: clear structure and activity but enigmatic function. Adv Enzyme Regul. 2008; 48:137–151. [PubMed: 18167316]

49. Zhai X, Malakhova ML, Pike HM, Benson LM, Bergen HR III, Sugár IP, Malinina L, Patel DJ, Brown RE. Glycolipid acquisition by human glycolipid transfer protein dramatically alters intrinsic tryptophan fluorescence: insights into glycolipid binding affinity. J Biol Chem. 2009; 284:13620–13628. [PubMed: 19270338]

50. Mesmin B, Pipalia NH, Lund FW, Ramlall TF, Sokolov A, Eliezer D, Maxfield FR. STARD4 abundance regulates sterol transport and sensing. Mol Biol Cell. 2011; 22:4004–4015. [PubMed: 21900492]

51. Pettersen EF, Goddard TD, Huang CC, Couch GS, Greenblatt DM, Meng EC, Ferrin TE. UCSF Chimera — a visualization system for exploratory research and analysis. J Comput Chem. 2004; 25:1605–1612. [PubMed: 15264254]

52. Lomize AL, Pogozheva ID, Lomize MA, Mosberg HI. Positioning of proteins in membranes: a computational approach. Protein Sci. 2006; 15:1318–1333. [PubMed: 16731967]

53. Sanner MF, Olson AJ, Spehner JC. Reduced surface: an efficient way to compute molecular surfaces. Biopolymers. 1996; 38:305–320. [PubMed: 8906967]

54. West G, Viitanen L, Alm C, Mattjus P, Salminen TA, Edqvist J. Identification of a glycosphingolipid transfer protein GLTP1 in *Arabidopsis thaliana*. FEBS J. 2008; 275:3421–3437. [PubMed: 18537822]

55. Zou X, Chung T, Lin X, Malakhova ML, Pike HL, Brown RE. Human glycolipid transfer protein (GLTP) genes: organization transcriptional status, and evolution. BMC Genomics. 2008; 9:72. [PubMed: 18261224]

NIH-PA Author Manuscript
NIH-PA Author Manuscript
NIH-PA Author Manuscript

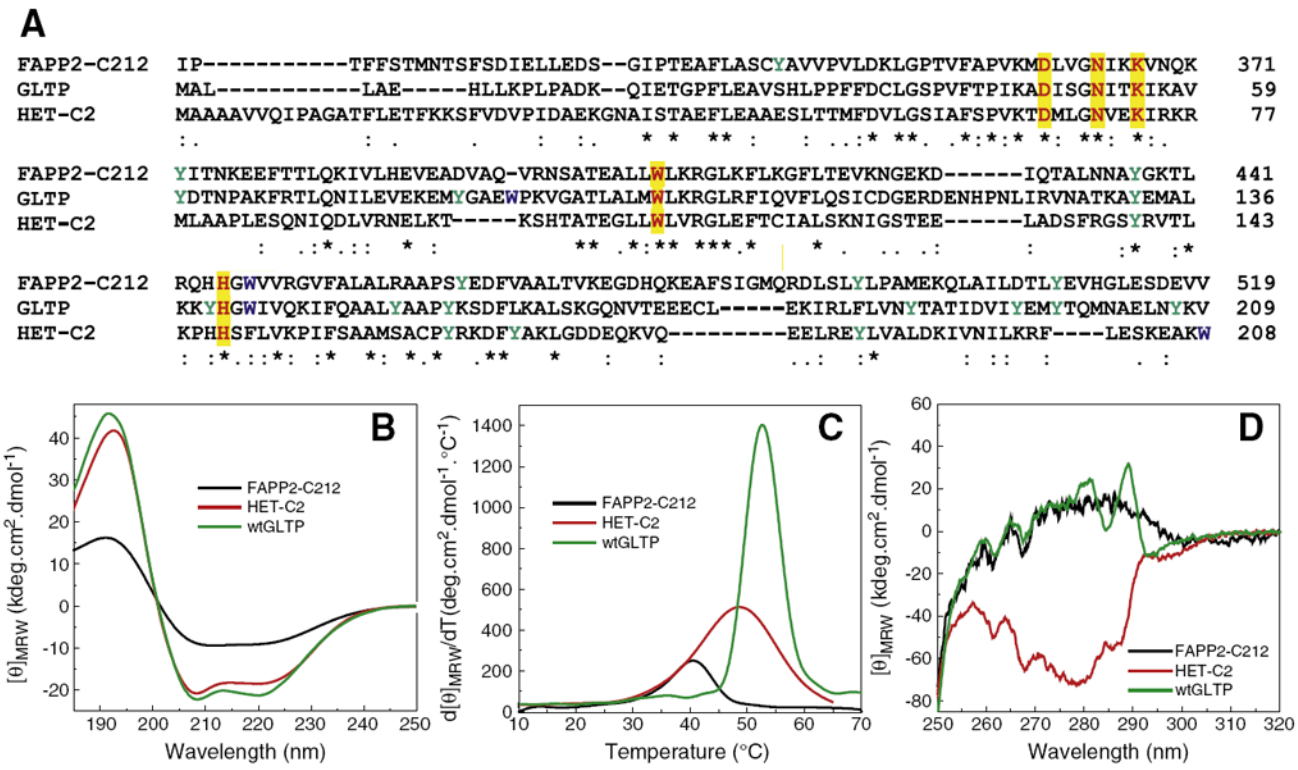

Fig. 1.

Sequence alignment of the C-terminal domain of FAPP2 with human GLTP and fungal HET-C2 and comparison of their conformation and stability by circular dichroism (CD). A) Sequence homology determined by T-coffee analysis (ver. 7.44). Highlighted yellow residues are key conserved residues involved in sugar headgroup binding of glycolipids. B) Far-UV CD spectra are presented in units of molar ellipticity per residue. The high helical content is indicated by the large negative n–π* transition at 222 nm as well as π–π* transition that splits into two transitions because of exciton coupling resulting in negative bands at ~208 nm and positive bands at ~192 nm. C) Temperature dependence of molar ellipticity at 222 nm (derivative plot). D) Near-UV CD spectra. Signals from Tyr (e.g. ~280 nm trough) and Trp (~288 nm trough) are not clearly discernible in FAPP2-C212.

NIH-PA Author Manuscript
NIH-PA Author Manuscript
NIH-PA Author Manuscript

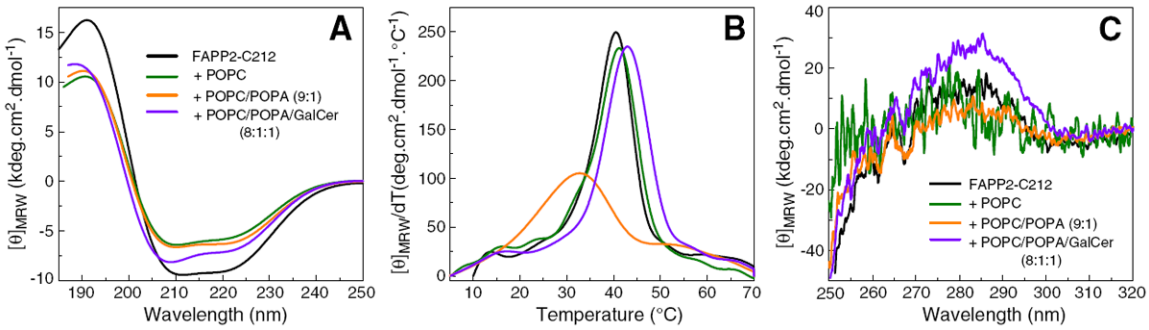

Fig. 2.

Conformational changes induced in FAPP2-C212 by vesicles with differing lipid composition assessed by far-UV and near-UV CD. FAPP2-C212+no vesicles (black); +POPC vesicles (green); +POPC/POPA (9:1) vesicles (orange); +POPC/POPA/18:1-GalCer (8:1:1) vesicles (purple). A) Far-UV CD spectra are presented in units of molar ellipticity per residue. Dramatic change in the secondary structure of FAPP2-C212 upon interaction with POPC, POPC/POPA, and POPC/POPA/18:1-GalCer vesicles is not observed. B) Temperature dependence of molar ellipticity at 222 nm (derivative plot). C) Near-UV CD spectra. Signal response from Tyr and Trp in FAPP2-C212 is not clearly discernible and changes induced by POPC, POPC/POPA, and POPC/POPA/18:1-GalCer vesicles are minor.

NIH-PA Author Manuscript
NIH-PA Author Manuscript
NIH-PA Author Manuscript

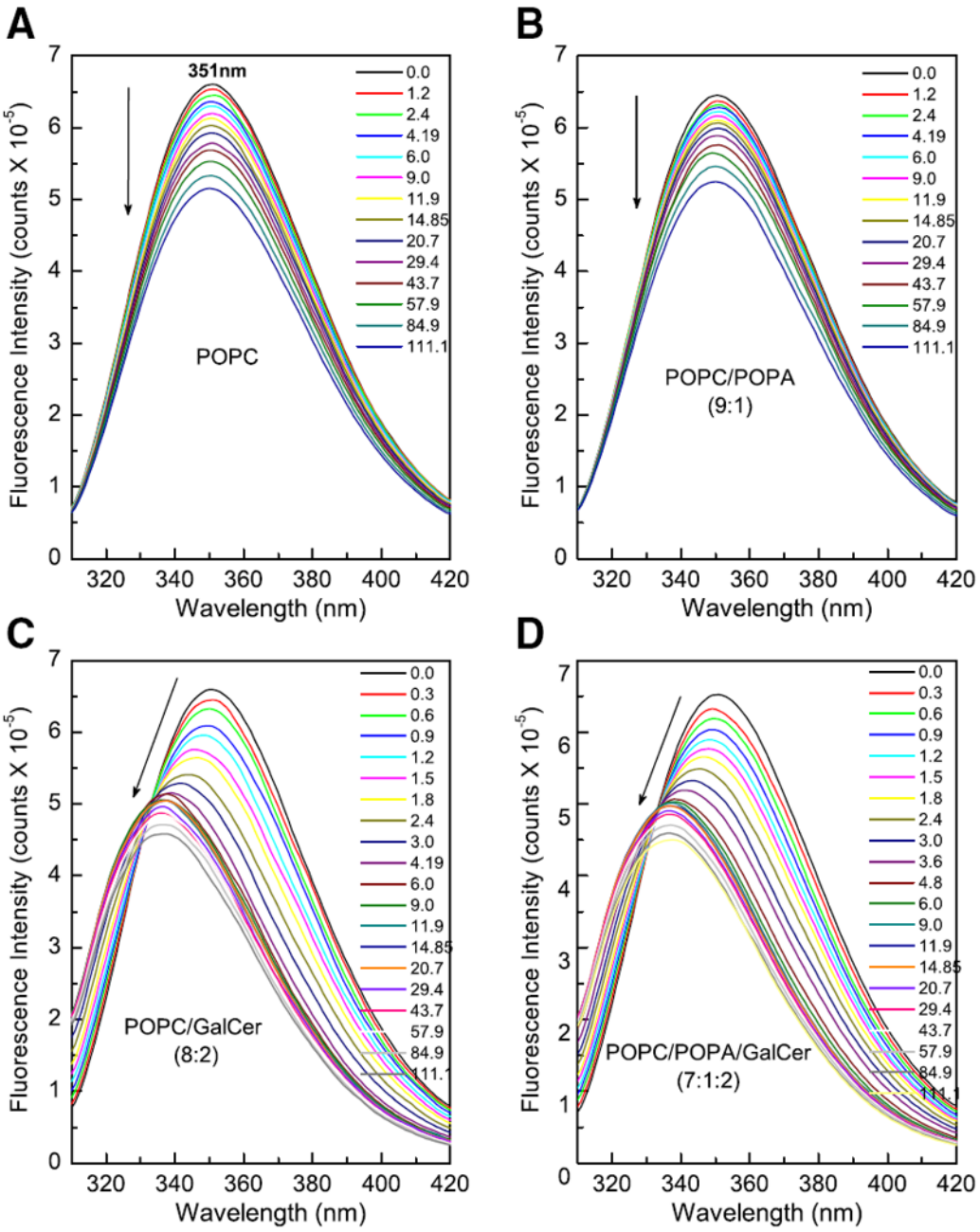

Fig. 3.

Changes in Trp emission of FAPP2-C212 induced by membrane lipids. A) POPC vesicles +FAPP2-C212; B) POPC/POPA (9:1) vesicles+FAPP2-C212; C) POPC:GalCer (8:2) vesicles+FAPP2-C212; D) POPC/POPA:GalCer (7:1:2) vesicles+FAPP2-C212. POPC and POPC/POPA vesicles lacking glycolipid induce no λ_{max} blue-shift and produce incremental intensity decreases (nonsaturable response). POPC and POPC/POPA vesicles containing glycolipid (GalCer) induce large λ_{max} blue-shift and strong initial intensity decrease (saturable response). Note that by the 9th addition (~4.2–4.8 μM glycolipid), the λ_{max} blue-shift ceases in panels C & D. However, with further vesicle injections, Trp emission intensity continues to decrease, as also is the case for POPC vesicles lacking glycolipid.

NIH-PA Author Manuscript

NIH-PA Author Manuscript

NIH-PA Author Manuscript

Glycolipid availability in the donor vesicle outer surface was estimated based on ~60/40 distribution between the outer and inner surfaces of vesicles [40,49].

NIH-PA Author Manuscript
NIH-PA Author Manuscript
NIH-PA Author Manuscript

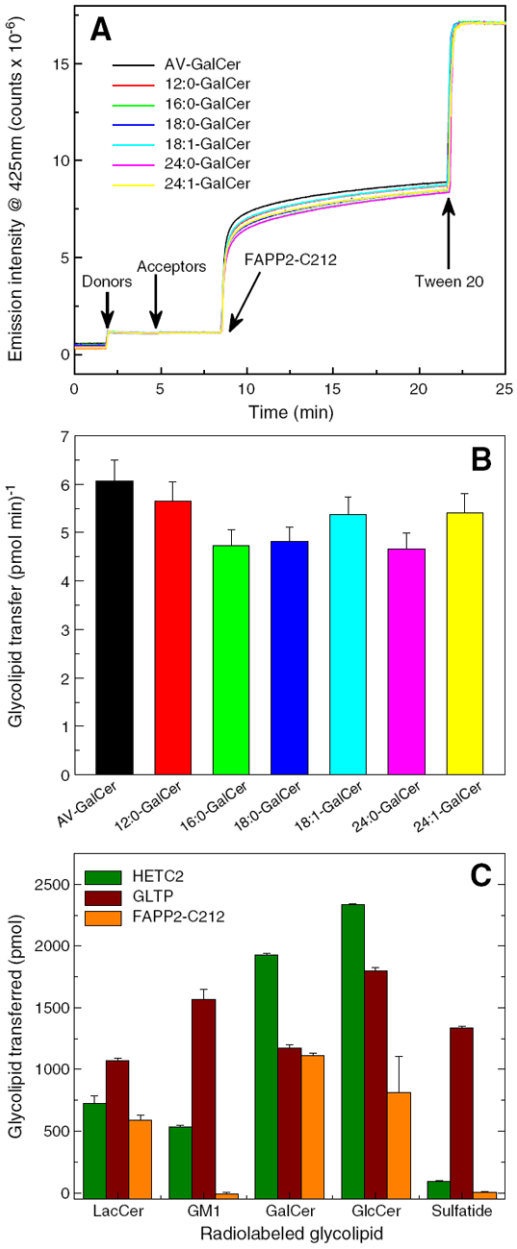

Fig. 4.

Glycolipid transfer activity of FAPP2-C212. Förster resonance energy transfer involving fluorescently-labeled glycolipid (AV-GalCer) and phospholipid (perylenoyl-PC) enabled assessment of glycolipid intervesicular transfer by FAPP2-C212. AV-GalCer was excited at 370 nm and emission wasmonitored at 425 nm. Additional details are provided in the Materials and methods section. A) Competition effect exerted by GalCer species with different homogenous acyl chains on AV-GalCer transfer by FAPP2-C212. B) Initial transfer rates for AV-GalCer measured in the presence of competitor GalCer species with different homogenous acyl chains. C) FAPP2-C212 glycolipid specificity. Glycolipid transfer activitywas measured at 30 °C using POPC donor vesicles containing radiolabeled glycolipid (2 mole%) and 10 mole% phosphatidic acid mixed with POPC acceptor vesicles (10-fold excess) and FAPP2-GLTP (0.5 μg). Recovery of acceptor vesicles eluting through

DEAE minicolumns enabled quantitation of glycolipid transfer by liquid scintillation counting as described in the Materials and methods section.

NIH-PA Author Manuscript
NIH-PA Author Manuscript
NIH-PA Author Manuscript

NIH-PA Author Manuscript
NIH-PA Author Manuscript
NIH-PA Author Manuscript

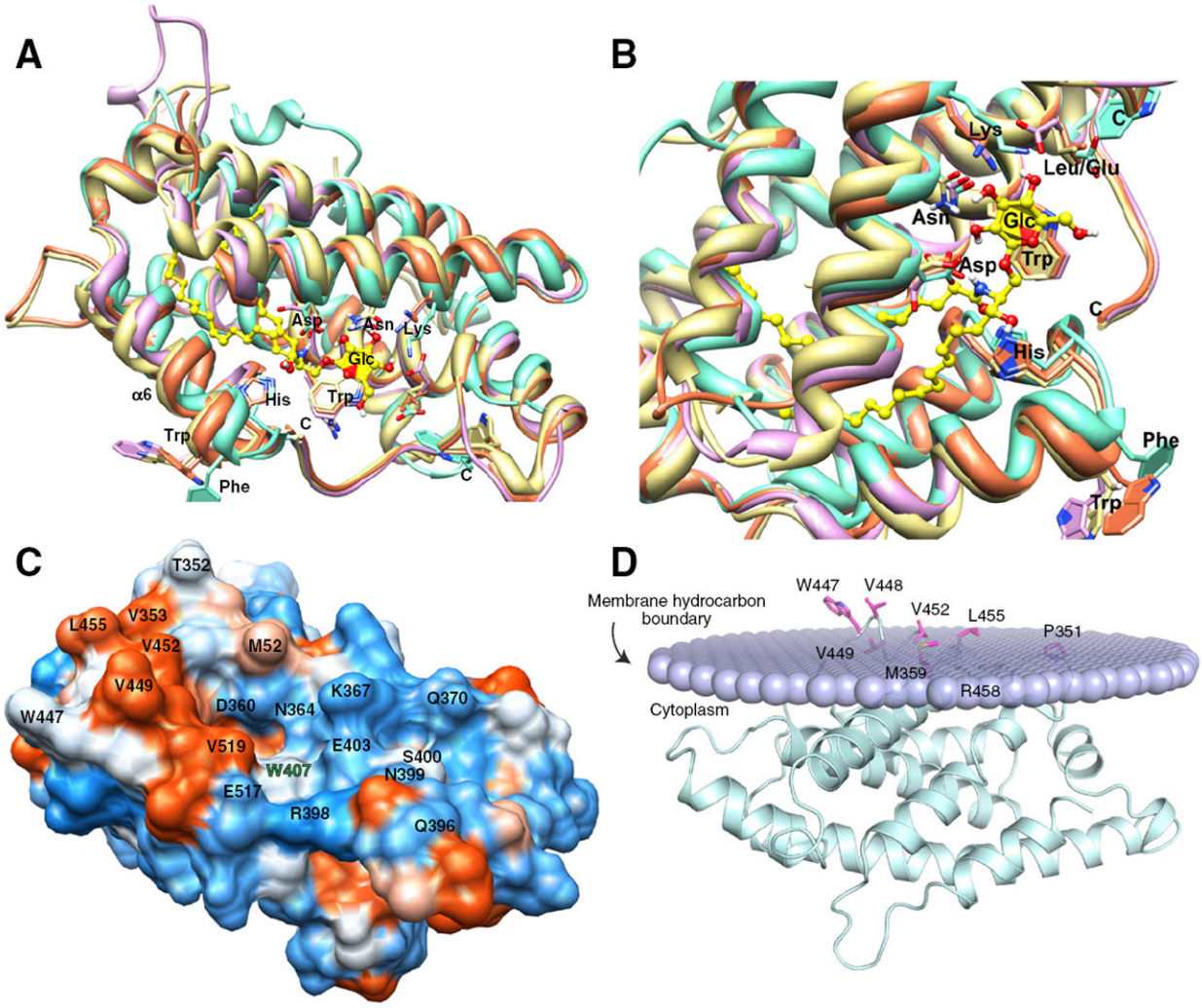

Fig. 5.

Structural homology modeling of FAPP2-C212, surface hydrophobicity, and predicted orientation during membrane docking. A) Structural homology modeling performed using the 3D-Jigsaw comparative modeling algorithm [34], which builds three-dimensional protein models based on homologues of known FAPP2-C212 structure is colored lavender; HET-C2, turquoise; apoGLTP, coral; holoGLTP, beige; (GLTP = PDB ID:1SWX & 3S0K; HET-C2 = PDB ID:3KV0). B) Zoom view of glycolipid binding site in A) following left-hand rotation of ~90°. Color scheme is same as in A). C) Surface hydrophobicity of FAPP2-GLTP mapped using Chimera (51), which relies on the Kyte–Doolittle scale to rank amino acid hydrophobicity, with blue indicating most hydrophilic (charged), white equaling 0.0, and orange-red being most hydrophobic. D) FAPP2-C212 orientation and positioning during membrane docking. The OPM computational approach (52) was used to identify residues involved in the initial docking of FAPP2-GLTP with the membrane interface. The lipid polar headgroups comprising half of the membrane are shown as lavender-colored. Not depicted are the lipid hydrocarbon chains which would project above the headgroups. FAPP2-C212 helices are cyan-colored, and membrane embedded side chain residues are shown in magenta. The membrane embedded residues are Pro^{351}, Met^{359}, Trp^{447}, Val^{448}, Val^{449}, Val^{452}, Leu^{455}, and Arg^{458}. The penetration depth into the bilayer is estimated to be ~5.8±0.8 Å with a tilt angle of ~87.±3° and $\Delta G_{transfer}$=−9.8 kcal/mol.

NIH-PA Author Manuscript
NIH-PA Author Manuscript
NIH-PA Author Manuscript

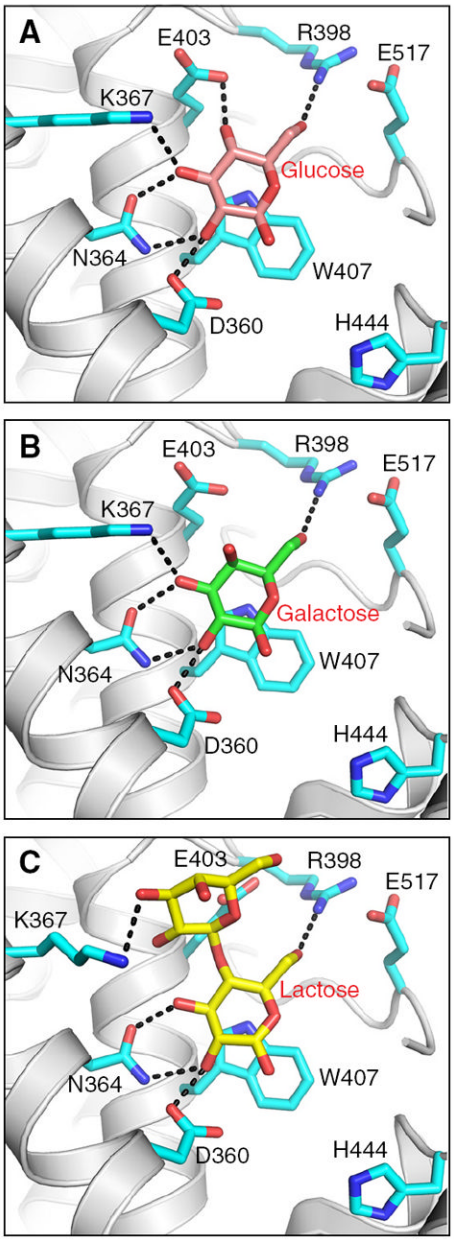

Fig. 6.

Docking of sugars into the FAPP2-C212 glycolipid headgroup surface recognition center. A) Docking of glucose. Side chains of FAPP-C212 residues involved in Glc binding are shown in cyan. The Glc sugar ring is colored cameo with red balls representing oxygen. The black dotted lines represent hydrogen bonds. B) Docking of galactose. The color scheme is the same as for A) except that the Gal sugar ring is colored green. C) Docking of lactose. The color scheme is the same as for A) except that the Lac sugar ring is colored yellow. The glucose, galactose, and lactose locations are derived from PDB IDs 3S0K, 2EVL, and 1SX6, respectively [15,16,42].

NIH-PA Author Manuscript

NIH-PA Author Manuscript

NIH-PA Author Manuscript

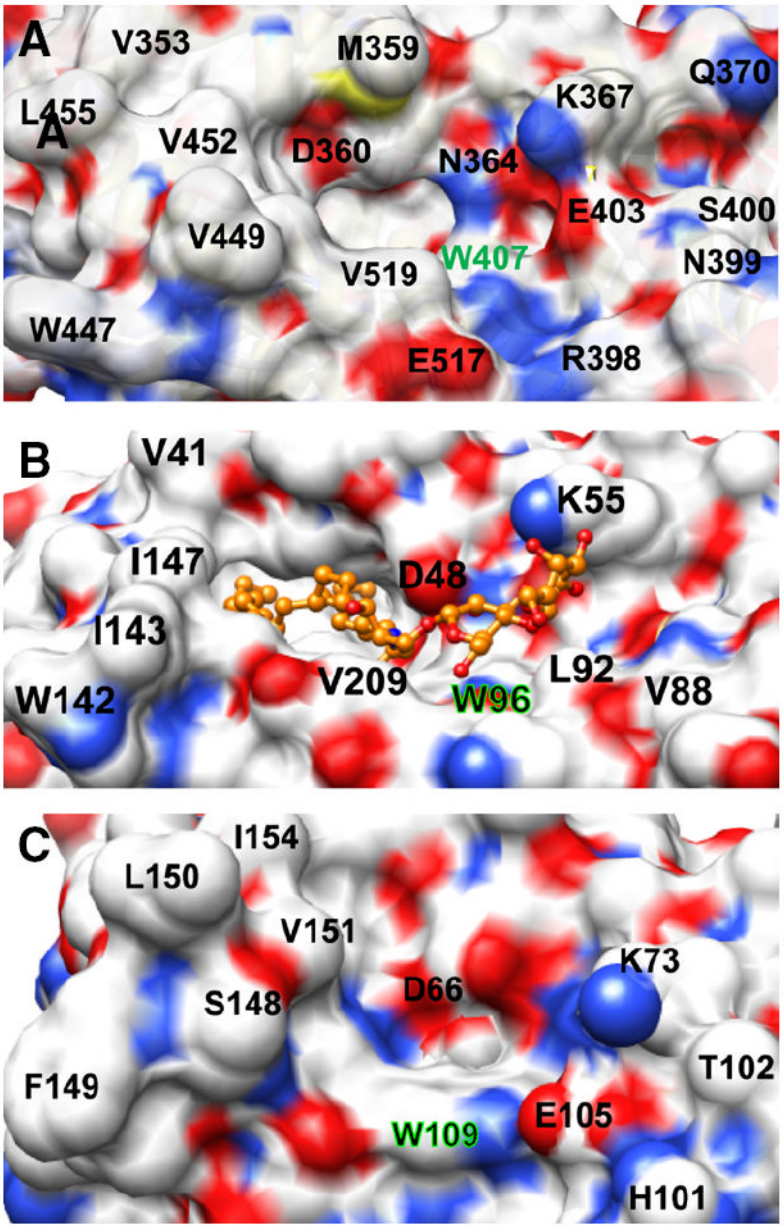

Fig. 7.

Surface topology of the sugar headgroup recognition site of FAPP2-C212, GLTP, and HET-C2. Surface residue color reflects the charge status (red = negative, blue = positive, and white = neutral). The Trp residue that interacts directly with the initial ceramide-linked GSL sugar in each GLTP-fold is accentuated by green highlights. A) FAPP2-C212. Residues such as Glu^{403}, Val^{519}, Val^{397}, Arg^{398}, Asn^{399}, and Ser^{400} partially obstruct the surface near Trp^{407} and constrict the sugar headgroup binding site. B) Human GLTP (PDB ID: 1SX6). 18:1-LacCer is depicted in gold with the ceramide hydrocarbon chains (left side) disappearing into the hydrophobic pocket. The open, unobstructed surface adjacent and to the right of Trp^{96} allows for broader selectivity for binding of various glycolipids. C) Fungal HET-C2 (PDB ID: 3KV0). Residues such as Glu^{105}, Thr^{102}, His^{101}, and Trp^{208} adjacent to Trp^{109} act as obstructions and create a pit-like sugar headgroup binding site.

NIH-PA Author Manuscript
NIH-PA Author Manuscript
NIH-PA Author Manuscript

Table 1

Secondary structure of FAPP2-C212 calculated from far-UV CD data in the presence and absence of lipid (with or without 18:1-GalCer).

Protein±liposome (SUV)	Helix 1*	Helix 2*	Strand 1*	Strand 2*	Turns	Unordered
FAPP2-C212	0.150	0.111	0.135	0.093	0.217	0.295
+POPC	0.073	0.089	0.206	0.111	0.212	0.309
+POPC/POPA	0.077	0.093	0.187	0.109	0.217	0.317
+POPA/POPA/18:1 GalCer	0.085	0.103	0.180	0.106	0.205	0.321

1* refers to regular; whereas, 2* refers to distorted [see 44,45 and references therein].

NIH-PA Author Manuscript

NIH-PA Author Manuscript

NIH-PA Author Manuscript

Table 2

K_d values of FAPP2-C212 for SUV vesicles.

Vesicle lipid composition	Partition coefficient K_d (μM)
POPC	10.61±0.80
POPC/18:1GalCer (8:2)	1.01±0.12
POPC/POPA (9:1)	13.48±2.51
POPC/POPA/18:1GalCer (7:1:2)	1.35±0.15

NIH-PA Author Manuscript

NIH-PA Author Manuscript

NIH-PA Author Manuscript

Table 3

Tryptophan fluorescence changes in FAPP2-C212 induced by interaction with POPC, POPC/18:1-GalCer, POPC/POPA and POPC/POPA/18:1-GalCer vesicles.

Vesicle lipid composition	Intensity	Blue-shift
+POPC	22%↓	1 nm
+POPC/18:1GalCer	30%↓	14 nm
+POPC/POPA	19%↓	1 nm
+POPC/POPA/18:1GalCer	31%↓	14 nm